Redox Interaction between Selenite and Mackinawite in Cement Pore Water

Kaifeng Wang, Alejandro Fernandez Martinez, Laura Simonelli, Benoit Madé, Pierre Hénocq, Bin Ma, Laurent Charlet

Redox interaction between selenite and mackinawite in cement pore water

Kaifeng Wang [1,2], Alejandro Fernandez Martinez[1], Laura Simonelli[3], Benoit Madé[4], Pierre Hénocq[4], Bin Ma[1,5*], Laurent Charlet[1*]

[1] University of Grenoble Alpes and CNRS, ISTerre, BP 53, 38041 Grenoble Cedex 9, France

[2] Engineering Technology Center of Decommissioning and Remediation, China Institute of Atomic Energy, 102413 Beijing, China

[3] BL22 – CLAESS, ALBA Synchrotron Light Source, 08290 Barcelona, Spain

[4]ANDRA, 1/7 rue Jean Monnet, Parc de la Croix Blanche, 92298 Chatenay-Malabry Cedex, France

[5] Laboratory for Waste Management, Nuclear Energy and Safety, Paul Scherrer Institute, 5232, Villigen, Switzerland

*Corresponding authors: charlet38@gmail.com, bin.ma@psi.ch

Abstract

In cement-rich radioactive waste repositories, mackinawite (FeS) could form at the steel corrosion interface within reinforced concrete and potentially retard the transport of redox-sensitive radionuclides (e.g., ^{79}Se) in cement porous media. Redox interactions between selenite and mackinawite in hyperalkaline conditions remain unclear and require further investigations. Here, using a comprehensive characterization on both aqueous and solid speciation, we successfully monitored the whole interaction process between selenite and mackinawite in hyperalkaline conditions. Results show similar chemical environments for SeO_3^{2-} and S^{2-}/S_n^{2-} at the mackinawite-water interface, verifying an immediate reduction. After 192 h reaction, SeO_3^{2-} was reduced to Se^0 and SeS_2, accompanied by the oxidation of S^{2-}/S_n^{2-} to $S_2O_3^{2-}$ and Fe(II) to Fe(III) in mackinawite. Aqueous results showed that ~99 % of aqueous selenium was present as Se_4S nano-particles due to the dissolution of Se from the solid. In parallel, ~62% of S^{2-}/S_n^{2-} was released into the solution, with mackinawite transforming to magnetite, $Fe(OH)_3$ and $FeS_2O_3^+$ complexed to Cl^- or OH^- species, and magnetite subsequently dispersed in the solution. This study provides valuable data about the retardation mechanisms of redox-sensitive radionuclides by soluble iron sulfides, which is critical to advance our understanding on reactive concrete barriers used in nuclear waste disposal systems.

Synopsis: The comprehensive investigation of the fate of Se, S and Fe under hyperalkaline conditions promotes a better description of cement-rich radioactive waste repository environments.

Key words: mackinawite, selenite, cement pore water, interaction mechanism, reactant fate

Table of Contents (TOC)

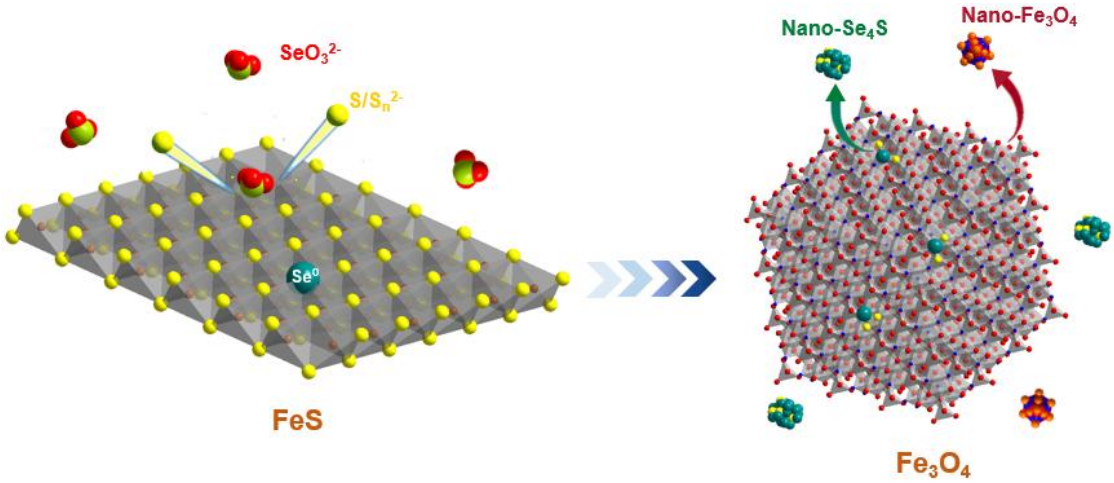

1. Introduction

The trace element selenium (Se) is essential for human health, but highly toxic when exceeding the appropriate intake range.[1] ^{79}Se is one of the ^{235}U fission products, with a long half-life of 4.8 $\times 10^5$ years. Its safe disposal is a requisite to the sustainable development of nuclear industry. Oxidized species of selenium are highly mobile, which has stimulated the research on selenium interactions with potential anthropogenic or natural barriers such as clays[2-4], cements[5-7] or Fe phases[4, 8-12]. The various oxidation states of selenium (-II, -I, 0, +IV, +VI) and their complexation ability with inorganic and organic matter make selenium chemistry complex. Under oxidizing conditions, Se often occurs as highly soluble and thus mobile oxyanionic forms, i.e., SeO_3^{2-} and SeO_4^{2-}. In contrast, under reducing conditions selenium adopts oxidation states of 0, -I and -II, having much lower solubility and mobility. This makes reductive immobilization an important pathway to decrease Se transport in the environment. Determining the ability of different barrier materials to reduce selenium species is therefore of high importance for the safety assessment of radioactive waste disposal initiatives.

The CEM-V/A cement, highly resistant to sulfate corrosion, is being evaluated as an engineered barrier for deep underground radioactive waste disposal in France. Mackinawite (FeS), a precursor of thermodynamically more stable iron sulfides minerals (e.g., greigite and pyrite), can be present naturally in host rocks of claystone and granite, and also in engineered concrete structures, such as at steel corrosion interfaces.[13] Its high reactivity and large specific surface area lead to a high potential to immobilize soluble ions, e.g., heavy metals and radionuclides[14-18]. Previous studies have shown that Se(IV) can be reduced to a tetragonal FeSe-like phase after being in contact with mackinawite under acidic and anoxic conditions. However, red Se(0) nanoparticles could be formed though the reduction of Se(IV) by mackinawite at higher pH.[10] Along with the Se(IV) reduction, mackinawite was oxidized to green rust firstly and then to magnetite or goethite. Besides, both aqueous Fe(II) and S(-II) were able to reduce Se(IV) to Se(0) under highly alkaline conditions (e.g., at pH ~13.29)[19]. Meanwhile, other studies observed that Se(IV) could be reduced to elemental Se or Se-S precipitates (e.g. Se_nS_{8-n}) by aqueous sulfide species. [20] However, to the best of our knowledge, little data on selenite sorption on mackinawite in the presence of cement pore water (at high pH) has been reported in literature. More specifically, precise information about the detailed interaction mechanism and the fate of each reactant in abiotic reduction processes by mackinawite under hyperalkaline conditions have not been fully unravelled. Considering that the geochemistry of selenite has close relationship with the chemical cycles of iron and sulfur in cement-rich repositories, a deeper knowledge about the interplay between selenite and mackinawite under the chemical environment of underground concrete structures (i.e., hyperalkaline and reducing conditions) is strongly required.

In this study, we have investigated the interaction mechanism between SeO_3^{2-} and mackinawite in cement pore water (CPW), the solution from the interconnected pore structure produced by cement hydration, using a combination of X-ray absorption spectroscopy (XAS), X-ray photoelectron spectroscopy (XPS), transmission electron

103 microscopy (TEM) and wet chemistry methods. This work contributes to advance the
104 understanding on the interaction mechanisms between redox-sensitive radionuclide
105 oxyanions and iron sulfides and to promote our knowledge on redox chemical
106 processes within reactive concrete barriers.

107 2. Materials and Methods

108 **2.1 Materials and Chemicals.** All chemicals used for synthesis of mackinawite (FeS)
109 and stock solution (CPW) were analytical reagents. Boiled and N_2-degassed Milli-Q
110 water (18.2 MΩ·cm) was used for all solutions and suspensions. Sodium selenite
111 ($Na_2SeO_3 \cdot 5H_2O$) and chemicals used for FeS synthesis and stock solution were
112 purchased from Sigma–Aldrich. Synthetic fresh CPW at pH ~13.5 according to the
113 recipe from CEA[21] was used as matrix solution in all reactors, with its chemical
114 composition shown in Table S1. All experiments were performed in a 99.99%
115 N_2-filled glovebox (O_2 < 2 ppm, using NaOH as the CO_2 trap) to prevent oxidation
116 and possible CO_2 contamination. The mackinawite suspension was prepared
117 following the method reported previsouly[10]. More details are shown in Text S1 of the
118 Supporting Information. The synthesized mackinawite solid was prepared on a silicon
119 plate, sealed in the air-tight powder holder, and then checked by powder X-ray
120 diffraction (XRD) (Bruker axs, D8 advance) with Vortex-EX detector (Hitachi) under
121 Cu Kα radiation, showing no distinct impurity diffraction peak (Figure S1). The
122 specific surface area of mackinawite was determined to be 102.3 m^2/g by the
123 Brunauer−Emmett−Teller (BET) N_2 absorption method. The surface site density was
124 assumed to be 4 site nm^{-2} and thus the corresponding surface-site concentration was
125 1.36 mM. The size and shape of the mackinawite particles were further characterized
126 by TEM as illustrated in Figure S2.

127 **2.2 Wet chemistry experiments.** Sorption experiments of SeO_3^{2-} on mackinawite
128 were performed at 25 °C under constant shaking and anoxic conditions (< 2 ppm O_2).
129 The system was tightly closed, except during sampling, to avoid CO_2 contamination.
130 The solid-to-liquid (S/L) ratio in all the reaction suspensions was set to 2 g/L. The

initially added concentration of SeO_3^{2-} was 4.70 mM. Prior to introducing SeO_3^{2-}, mackinawite was equilibrated with CPW for 24 h. The pH of suspension was measured by a combined glass Micro-pH electrode (Metrohm 6.0234.100) during the reaction after its calibration by pH 4.00, 7.01, 10.00 and 12.00 standard solutions. A combined Pt-ring ORP electrode (Metrohm 6.0451.100) was used for the Eh measurement, after being calibrated with Zobell's solution (200 mV at 25 °C).[22] Samples of 10 mL of the suspension were filtered by 0.22 μm nitrocellulose membrane by vacuum filtration at reaction times of 1, 17, 24, 50, 73, 96, 138 and 192 hours. Extreme care was taken to minimize the potential for sample oxidation during subsequent solid characterizations (see the details in Text S2). Total aqueous concentrations of S, Fe and Se in the filtrates were analyzed by inductively coupled plasma optical emission spectrometry (ICP-OES) with a Varian 720-ES apparatus. The concentrations of SeO_3^{2-} and sulfur species, including S^{2-}/S_n^{2-}, SO_3^{2-} and SO_4^{2-}, were analyzed by ion chromatography (Dionex ICS-6000) with an Dionex™ IonPac™ AS9-HC IC Columns with 0.8 mL/min Na_2CO_3 (12.5 mM) as eluent. The retention time and calibration curves for SeO_3^{2-} and sulfur species were shown in Figure S3 and the standards of IC were cross-checked by ICP-OES.

2.3 X-ray Absorption Spectroscopy (XAS). Iron and selenium K-edge X-ray absorption near-edge structure (XANES) and extended X-ray absorption fine structure (EXAFS) spectra were collected at the Core Level Absorption & Emission Spectroscopy (CLÆSS, BL22) beamline at the Spanish synchrotron ALBA-CELLS, Barcelona, Spain. Elemental Se foil and Fe foil were used for energy calibrations in parallel with the measurements at the Se K-edge (12.658 keV) and Fe K-edge (7.112 keV), respectively. Si(111) and Si(311) double crystal monochromators were used with approximately 0.3 eV resolution at 2.5 keV. A silicon drift detector (KETEK GmbH AXAS-M with an area of 80 mm^2) was employed to collect the fluorescence signal. All the samples for XAS were double-face sealed using polyimide tape, mounted on a sample holder, and measured in fluorescence mode, except for Se and

Fe references, which were prepared as pellets with a cellulose matrix and measured in transmission mode. Before being transferred into the vacuum experimental chamber, samples were stored under N_2 atmosphere. For EXAFS signal collection, a liquid N_2 cryostat was used to lower the temperature to 77 K, in order to minimize the effects of thermal disorder due to atomic vibrations. The data integration and reduction of XANES and EXAFS spectra were performed by the Demeter software package.[23] Linear combination fits (LCF) were applied to identify and quantify the components in samples. Regarding the quantitative EXAFS fit of Se samples, radial distribution functions were obtained by Fourier Transform (FT) of k^3-weighted EXAFS oscillations (k-range: 3.0–12.0 $Å^{-1}$) using a Kaiser-Bessel window. FEFF8.4 was used to calculate the theoretical backscattering paths to perform the fits of radial distribution functions.[24] Only the first atomic shell ($R+\Delta R$: 1.0–2.7 Å) was fitted considering the quality of the EXAFS data.

2.4 Transmission Electron Microscopy (TEM). The pristine mackinawite, as well as the solids and nano-sized colloids after reaction, were analyzed by TEM (JEM-2100F) with energy dispersive X-ray spectroscopy (EDS). The solid samples were dispersed in ethanol and sonicated for 5 min, while no treatment was performed for the supernatant. A drop of treated samples was deposited on ultra-thin carbon grids for the measurement. TEM images were collected at 200 keV. Gatan Digital Micrograph software was used to analyze the images.

2.5 **X-ray photoelectron spectra (XPS)**. XPS was recorded with a Kratos Axis Ultra electron spectrometer equipped with a delay line detector. The reacted solid was collected and dried in the glove box and then brought to the XPS facility using an anaerobic jar. To avoid any oxidation, the samples were quickly transferred to the XPS chamber. A monochromatic Al Kα source operated at 150 W, a hybrid lens system with a magnetic lens providing an analysis area of 0.3 mm × 0.7 mm, and a charge neutralizer were employed for the measurement. The energy step was set to 0.1 eV for collecting Fe and S data. The binding energy was always calibrated using

C 1s peak (284.8 eV). The XPS spectra of Fe 2p and S 2p were fitted using the CasaXPS software with Gaussian Lorentzian function through background-subtraction corrections using a Shirley-type optimization.

3. Results and Discussion

3.1 Selenium reduction kinetics

The pH of the suspension stayed constant for the entire duration of the experiment, whereas the Eh decreased during the first 50 h and then remained stable until 192h (Figure S4). The Eh decrease could result from the continuous consumption of oxidants (i.e., Se(IV)), in good accordance with the Se(IV) concentration decrease as shown in Figure 1. Aqueous concentrations of SeO_3^{2-} and total Se during the reaction with mackinawite are shown in Figure 1. Nearly all the aqueous SeO_3^{2-} was removed by mackinawite after 96 h. Specifically, during the first 24 h the aqueous concentration of total Se was equal to that of SeO_3^{2-}, indicating that SeO_3^{2-} was the only species in aqueous phase and that the decreased amount of SeO_3^{2-} was retained in the bulk solid phase. More intriguingly, after reacting for 50 h the aqueous concentration of SeO_3^{2-} continued to decrease while the total concentration of selenium as determined in the filtrate was increasing with reaction time. This suggests that the reduction products of SeO_3^{2-} could be nano-sized, such as nano-Se^0, resulting in a colloidal dispersion in the suspension, which could not be separated out by the 0.22 μm membrane. After reaction for 73 h, the concentration of Se(IV) decreased to 0.17 mM but the Se_{tot} concentration was 3.01 mM, which implied a concentration of 2.84 mM aqueous Se nanoparticles in the solution. Although previous studies also showed that mackinawite had an extremely strong affinity towards Se(IV), the formation of nano-Se^0 colloids has been rarely reported.[2,25,26] The distinct reaction kinetics and products observed here could be probably related to the hyperalkaline nature of CPW. The disassociation of nano-Se^0 from the solid adsorbent was likely to be accompanied with a dissolution of makinawite, which will be discussed afterwards in detail. Meanwhile, the filtrate colors turned yellow after 24 h reaction from

transparent (1 h) to orange (50 h), olive (73 h) and black (138 h and 192 h), as shown in Figure S5. The orange color at 50 h might suggest that SeO_3^{2-} was reduced to red Se^0 nanoparticles that were released to the solution afterwards. Han et al and Breynaert et al. also observed that the makinawite suspension turned red after interacting with Se(IV) regardless of the ratios of Se(IV)/FeS; they speculated that Se(0) particles formed through Fe-mediated Se(IV) reduction.[2, 25] Therefore, the total Se concentration of the filtrate took into account both aqueous SeO_3^{2-} and dispersed nanosized Se^0 species. At 192 h, the concentrations of Se_{tot} and Se(IV) measured in the filtrate were 4.40 mM and 0.031 mM, respectively, indicating that ~ 0.3 mM (6 %) of Se was adsorbed on the solid and ~99 % of aqueous Se was reduced species. The mass balance of Se in the filtrate (measured) and filtered solid (calculated) at different reaction times is listed in Table S4. Moreover, the filtrate color continued to change, and turned olive and black from 73 to 192h, indicating the possible formation of green rust and magnetite. This was due to the oxidation of FeS and the subsequent release of iron nanoparticles into the solution, which caused the increased of measured Fe concentrations (Figure 1). The chemical interactions between mackinawite and SeO_3^{2-} in CPW (pH ~13.5) were simulated by Phreeqc modelling using the Andra THERMOCHIMIE database.[27] The experimental aqueous Fe concentration (0.62 mM at 192 h) is comparable with but lower than the calculated values of 1.5 mM $Fe(OH)_3^-$ and 1.7 mM $Fe(OH)_4^-$, respectively. This is probably due to the lack of thermodynamic equilibrium. Note that the measured Fe concentrations in the filtrates also include the contributions from nano-sized magnetite as indicated by the dark colour of filtrates in Figure S5. The precise forms of Se-solid species were further explored using XAS.

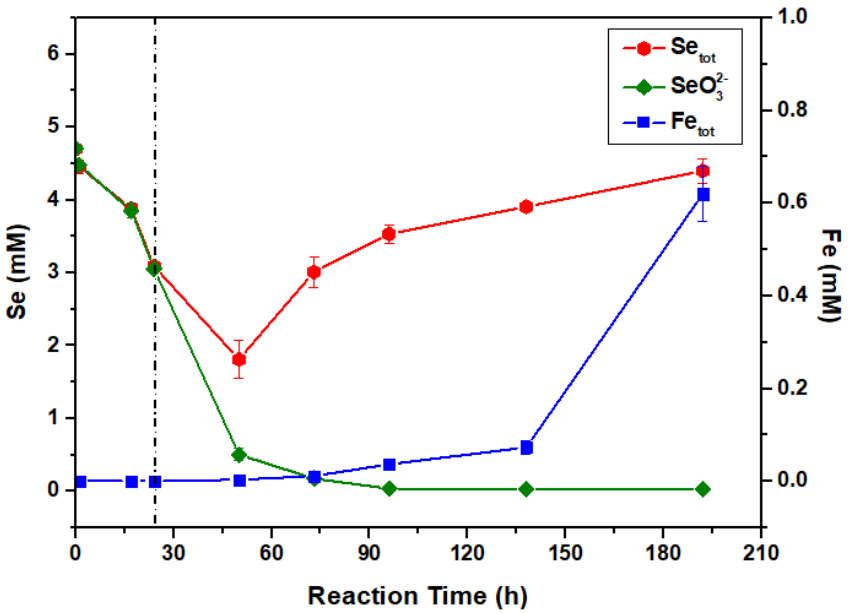

Figure 1. Measured concentration of SeO_3^{2-} by IC, total Se and Fe by ICP-OES in CPW as a function of the reaction time.

In XAS, the XANES region of the probed element can be used as a fingerprint of the chemical species, which depends both upon the valence state and the coordination environment. Se K-edge XANES spectra were collected for solid samples at different reaction times. LCF results of the solids and the references are shown in Figure 2. After reacting for 1 h, SeO_3^{2-} was mainly reduced into 35.8(3.0)% $FeSe_2$, 35.5(9.2)% FeSe and 19.2(1.0)% SeS_2, while only 4.9(2.9)% Se^0 and 4.9(1.2)% SeO_3^{2-} could be identified, indicating that SeO_3^{2-} can be quickly adsorbed on the surface and reduced to Se(0, -I, -II). From 24 h to 196 h, all the spectra showed similar features, with ~63% SeS_2 and 30-32% Se^0 identified to be the primary solid Se species. In contrast, previous studies at lower pH demonstrated that nano Se^0 was the main reduced Se product.[10, 19, 25]. Kang et al. found that Se(-II) was transformed to elemental Se in the presence of remaining non-reduced selenium oxyanions.[29] Therefore, the reduced species of FeSe and $FeSe_2$ after reacting for 1 h could be oxidized by the residual SeO_3^{2-} forming Se(0) at 24h and the corresponding reaction would be:

$$SeO_3^{2-}{}_{(aq)} + 2FeSe_{(s)} + 3H_2O \rightarrow 3Se^0{}_{(s)} + 2Fe(OH)_{2(cr)} + 2OH^-$$

EXAFS data were fitted to determine the coordination environments of adsorbed

selenium, as shown in Figure S6. Fitting the main peak in *R* space allowed obtaining interatomic distances and coordination numbers (CN) for the first two coordination shells. As shown in Table S2, the spectrum of the 1 h sample yielded a CN ~1.7 Se-Fe pair at 2.31 Å and CN ~1.1 Se-Se pair at 2.61 Å. The Se-Se backscattering path used was the average from the Se-Se paths of FeSe, $FeSe_2$, SeS_2 and Se^0. Regarding samples from 24, 73 and 192 h, apart from the Se-Se pair that was fitted at ~2.3 Å with a CN ~ 1.5, a backscattering signal from Se-S pair was also observed, resulting in a CN of ~0.6-0.9 with $d_{Se\text{-}S}$ = ~2.1 Å. The EXAFS fits also confirmed the existence of SeS_x species in the solid product. Diener et al. reported that selenium, belonging to the family of chalcophile, can incorporate into the structure of mackinawite and pyrite by replacing S sites and consequently forming zero-valent Se. Also, the decreased coordination number of the neighbour Se atoms around the incorporated Se^0 site indicated a small cluster size,[30] in good agreement with our study. With regard to the SeS_x precipitate, the zero-valence selenium and sulfur are miscible in all proportions and can form cyclic-structures (e.g. Se_nS_{8-n}). Previous studies have showed that Se_nS_{8-n} are susceptible to form and precipitate as a result of Se(IV) reduction by sulfide, though the resulting sulfur-to-selenium ratio varied from 1.7 to 2.3.[31] However, TEM imaging and EDS mapping analysis did not succeed in identifying Se^0 nanoparticles and Se-S precipitates on the surface of solid sample for 192 h (the expected shape of Se-S particles is irregular and the elemental Se can adopt nanospheres and nanorod-like morphologies).[32, 33] Furthermore, no obvious selenium peaks of 50 and 192 h filtered solids were checked by XRD probably due to the poor crystallinity or detection limit (Figure S7). The Se was therefore likely to be present forming very small precipitates or amorphous atomic level cooperation with S (Figure S8). By combining with the information from Se K-edge XANES results, we proposed that SeO_3^{2-} was adsorbed onto surface sites corresponding to the S^{2-}/S_n^{2-} environment of mackinawite, and it was reduced by neighboring S^{2-}/S_n^{2-} or Fe^{2+}, forming a very fine Se^0 phase or amorphous cluster followed by the formation of Se-S through the immediate bonding to Se^0 and S. The S^{2-}/S_n^{2-} that was substituted by

SeO_3^{2-} dissolved into the solution (see Section 3.2). The Eh-pH diagrams of Se and Fe species calculated using Andra THERMOCHIMIE database are shown in Figure S9. It is worth noting that after 192 h zero-valent Se predominated among Se species, even though ferroselite ($FeSe_2$) was predicted to be more stable under the experimental conditions of pH ~13.5 and Eh ~-0.4 V as indicated in Figure S9(a). The zero-valent Se is therefore a metastable phase, with slow transformation kinetics from Se^0 to Se(-I). These results allow making a hypothesis to explain the fact mentioned above: the total concentration of selenium was higher than that of SeO_3^{2-} after reacting for 24 h. It can be speculated here that ≡Fe-S-Se^0 could break down to its constituent parts in CPW, i.e. into ≡Fe-S and nano-Se^0, or ≡Fe-OH and nano-sized SeS species. After 192 h, the nanoparticles present in the filtrate were characterized by (S)TEM (Figure 3). As it can be seen, the size of nanoparticles was approximately ~20 to 60 nm (Figure 3a). The nanoparticles formed at 192 h consisted of Se, S, Fe and O with a ratio of Se to S roughly at 4:1 according to EDS analysis (Figure S10). Generally, elemental Se occurs in three forms: trigonal Se (t-Se), monoclinic Se (m-Se) and amorphous Se (a-Se). The interplanar spacings of trigonal Se that is considered as the most stable allotropic form are 4.96 Å and 3.78 Å along and perpendicular to the helicoid growth direction, respectively,[34] which was different from that (4.3 Å) observed in nanoparticles in the filtrate as shown in Figure 3b. Taking into account the EDS results, the interplanar spacing may belong to Se_4S crystalline phase, whereas no data is available to identify the lattice plane of Se_4S. Se species in the filtered solids and filtrates at different reaction times are shown in Table S3. The high-resolution transmission electron microscopy (HRTEM) image (Figure 3c) illustrated that the interplanar spacing was ~2.5 Å, corresponding to the (331) lattice plane of magnetite (Fe_3O_4).[35] This indicates that mackinawite transformed to nanosized magnetite during the reaction, resulting in the increased Fe concentration with time shown in Figure 1.

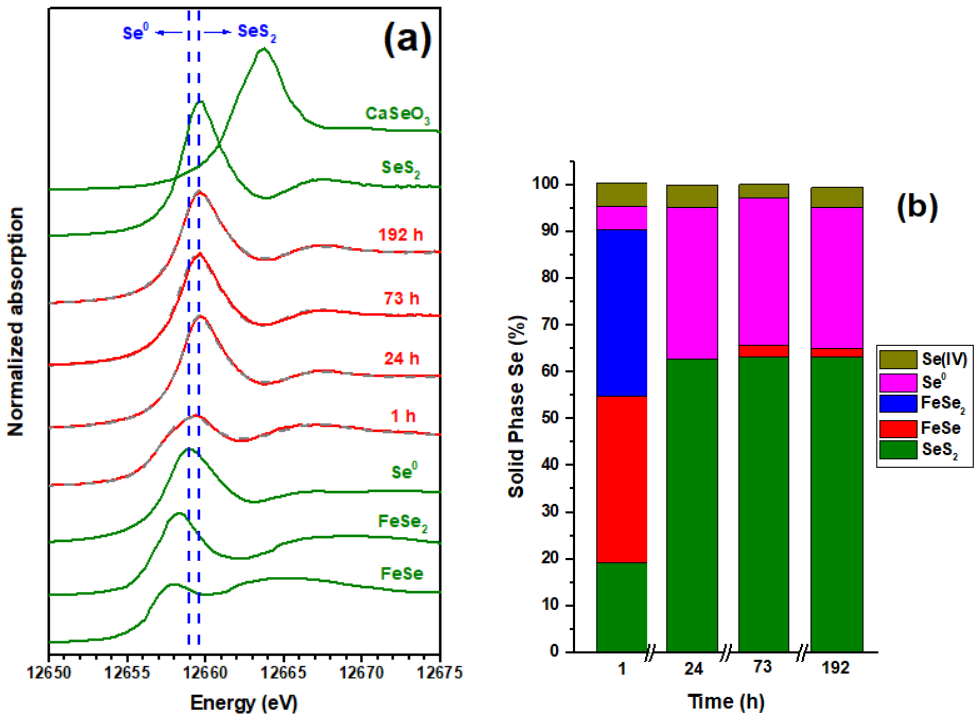

315

316 Figure 2. (a) Se K-edge normalized XANES spectra of solid samples after reacting for
317 1, 24, 73 and 192 h, comparing to Se references. (b) The fractions of FeSe, $FeSe_2$, Se^0,
318 SeS_2 and $CaSeO_3$ components in each Se-solid sample determined by LCF method.

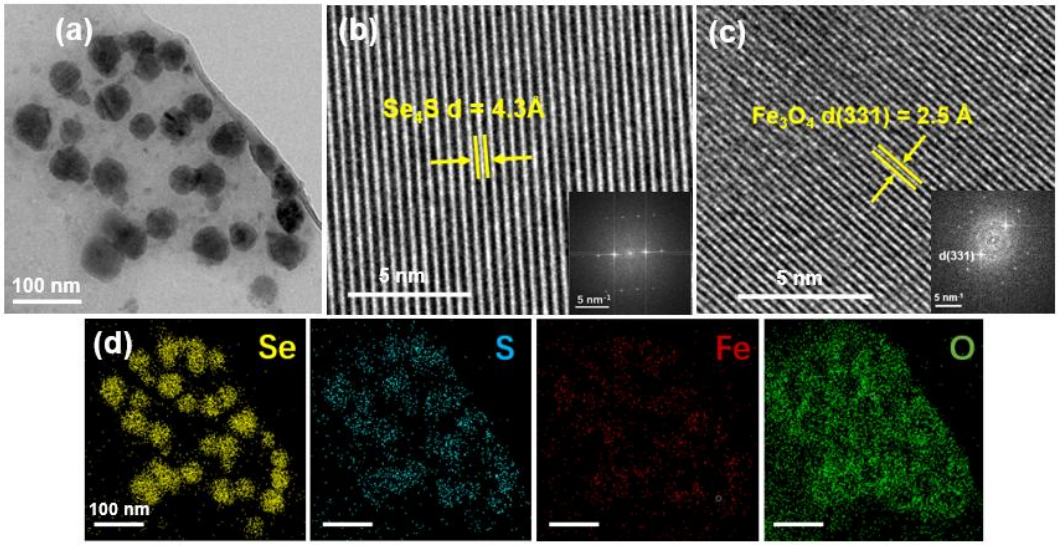

319

320 Figure 3. Transmission electron micrographs of nanoparticles found in the filtrate
321 after reaction for 192 h. (a) Transmission electron microscopy image; high resolution
322 transmission electron microscopy (HR-TEM) image on two spots on a single particle
323 (b) SeS_4 and (c) Fe_3O_4 with the corresponding Fast Fourier Transform (FFT); (d)

Elemental mapping by energy-dispersive X-ray spectroscopy analysis with Se in yellow, S in blue, Fe in red and O in green.

3.2. Dissolution kinetics of mackinawite with/without SeO_3^{2-}

The ion concentrations of CPW equilibrated with mackinawite for 24 hours are shown in Table S4. 1.28 mM Ca^{2+} was removed from the original CPW by mackinawite after 24 h equilibration, nearly equal to the value of the mackinawite surface-site concentration of (1.36 mM). The pH value (~13.5) of CPW was much higher that the point of zero charge of mackinawite (7.5).[36] It is reasonable to think thus that the negatively charged surface of mackinawite favored the adsorption of Ca^{2+} from CPW leading to the formation of $\equiv FeSCa^{2+}$ surface species. 0.24 mM S^{2-} and almost no Fe were detected after 24 h, suggesting that mackinawite was not congruently dissolved. However, Phreeqc calculations predicted that 0.06 mM of both HS^- and Fe^{2+} should be released once the dissolution reached equilibrium. A plot of S concentration versus reaction time is shown in Figure 4. It can be seen that when no SeO_3^{2-} was added, the S^{2-}/S_n^{2-} concentration increased very slowly and aqueous SO_4^{2-} (blank) was kept constant with increasing reaction time. This suggests a limited dissolution of mackinawite and no significant amount of aqueous SO_4^{2-} adsorbed onto mackinawite. The color of filtrate after 192 h was clear and the measured Eh of the suspension was about – 0.402 V, which is closed to the Eh value (-0.398 ± 0.005 V) of the suspension with SeO_3^{2-} (Figure S4). In contrast, in the presence of SeO_3^{2-}, a critical threshold of reaction time (73 h) was observed based on the concentration change of S^{2-}/S_n^{2-}. Dissolved concentration of S^{2-}/S_n^{2-} originating from the solid increased quickly during the first 73 h, remaining roughly constant at 13-14 mM thereafter; the same tendency for the total concentration of sulfur was observed. This supports the hypothesis that 2 to 3 S^{2-}/S_n^{2-} units were substituted by one SeO_3^{2-} atom according to the concentrations of the two species. The measured concentrations of SO_4^{2-}, S^{2-}/S_n^{2-}, SO_3^{2-} and total S with the addition of SeO_3^{2-} are shown in Table S6. After reaction for 1 h, the summation (1.74 mM) of SO_4^{2-}, S^{2-}/S_n^{2-} and SO_3^{2-} concentrations by IC was lower

than the total concentration of S (2.34 mM) by ICP. This suggests that other soluble S species, probably S^0, existed in solution. However, it is almost the same value between the total S concentration and the sum from 24 h to 192 h. It means that no other S species were present in the filtrates. 14.12 mM S^{2-}/S_n^{2-} was detected in the filtrate and the dissolution efficiency was ~62% after 192h. The mass balance of S in the filtrate (measured) and filtered solid (calculated) at different reaction times is listed in Table S4. Han et al. proposed a mechanism by which Se(IV) was reduced to FeSe or $FeSe_2$ by mackinawite at pH 8 and the replaced sulfide by Se released into the solution, with no detection of aqueous sulfide.[25] The SO_4^{2-} concentration remained 1.55 ± 0.03 mM during the reaction, which means that no SO_4^{2-} adsorbed on the surface of the solid during reaction. A considerable amount of aqueous SO_3^{2-} was observed following the same kinetic tendency of sulfide, resulting in 1.20 mM SO_3^{2-} after 192 h. SO_3^{2-} can be present as intermediate but stable species at high pH, as the presence of S^{2-} seems to inhibit further oxidation of SO_3^{2-}.[37]

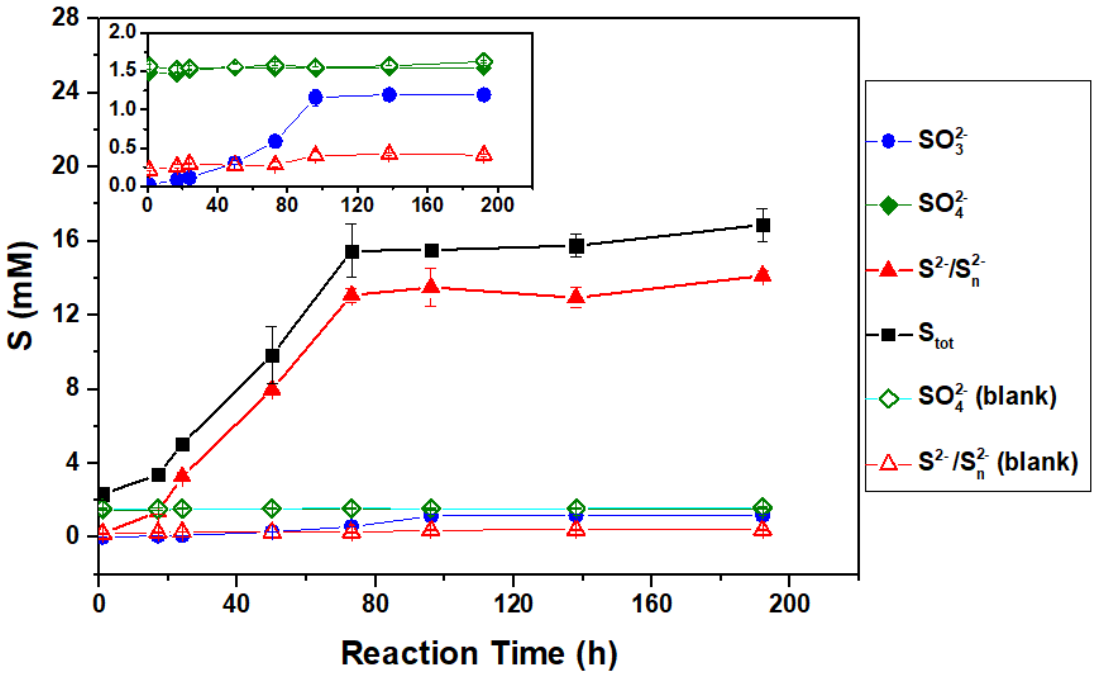

Figure 4. Measured concentration profiles of (poly)sulfide (S^{2-}/S_n^{2-}), sulfate (SO_4^{2-}) and sulfite (SO_3^{2-}) of the experiment with SeO_3^{2-} and S^{2-}/S_n^{2-} (blank), SO_4^{2-} (blank) of

experiment without SeO_3^{2-} as a function of reaction time. The inset shows an enlarged view of the less abundant species.

3.3 Possible Reaction Involving Fe, S and Se

S(2p) and Fe($2p_{3/2}$) XPS spectra of Se-reacted mackinawite nanoparticles at different reaction times are shown in Figures 5a and 5b. In Figure 5a, to adequately fit the S(2p) spectrum of pure mackinawite (0h), three $2p_{3/2}$ components at 160.9 eV, 162.7 eV and 164.4 eV were required. The one at 160.9 eV, accounting for 71.3% of the total S(2p) signal, was typically attributed to sulfide(S^2); the second component located at 162.7 eV may correspond to polysulfides (S_n^{2-}), taking up 27.3%. The third was fitted to take into account the high energy tail of the S(2p) spectrum, attributed to elemental sulfur S^0 (1.4%) (Table S7).[32] The S:Fe ratio of 1.2 derived from TEM-EDS analysis experiments was consistent with the data of previous studies,[42] and suggests the formation of greigite ($Fe_2^{III}Fe^{II}S_4$) on the surface of mackinawite, although this solid was not identified by XRD.[41] Recently studies revealed the existence of Fe_3S_4 species in FeS_{nano}, as a solid-phase precursor of mackinawite, and of edge-sharing FeS_4 species to stabilize FeS structure to form mackinawite.[43-44] In our case, we speculate that Fe_3S_4, as the representative species of solid S_n^{2-}, reacted with SeO_3^{2-} especially at 1 h. A set of redox and oxidation reactions susceptible to occur between Se couples and the considered solid product couples are listed in Table S8. After reacting with SeO_3^{2-}, the S(2p) spectra exhibited different features, which were characterized by the energy increases (0.6-0.7 eV) of S^{2-} and S_n^{2-} species and probably attributed to surface defects, Ca or Se impact. After 1 h reaction, there is evidence for thiosulfate ($S_2O_3^{2-}$) species at 168.0 eV by XPS and an obvious decrease of S_n^{2-} signal of solid coupled to an increase in S^0 and $S_2O_3^{2-}$ contributions, indicating that S_n^{2-} (Fe_3S_4) on the surface of mackinawite was oxidized to S^0 and $S_2O_3^{2-}$ accompanied with SeO_3^{2-} reduction to FeSe, $FeSe_2$ and Se^0 (Figure 2). The corresponding half reactions (1)-(5) are listed in Table S8. Oxidation reaction (4) and (5) suggest that S_n^{2-} ($Fe_2^{III}Fe^{II}S_4$) was the active reductant of aqueous SeO_3^{2-} within a short reaction

time and was responsible for the formation of FeSe and $FeSe_2$ at high pH via the formation of $Fe(OH)_2$ and $Fe(OH)_3$ species, which was also confirmed in acid solution.[45] Previous studies showed that SO_3^{2-} reacted with S^0 to form thiosulfate ($S_2O_3^{2-}$), which is thermodynamically stable and is an excellent complexing agent for metal ions.[38] Therefore, the $S_2O_3^{2-}$ species detected in our system were probably formed though the disproportionation reaction. Also, $S_2O_3^{2-}$/$S_4O_6^{2-}$ was observed in the reaction between Se(IV) and pyrite by Han et al.,[39] while Scheinost et al. reported that the sulfide in mackinawite was oxidized to elemental sulfur at pH 5.7, coupled to the reduction of Se(IV).[40] The content of S^{2-} decreased from 67.6% at 1 h to 36.1% after 24 h contact, while an increase of S_n^{2-} and $S_2O_3^{2-}$ content occurred simultaneously. As the oxidation state S within S^{2-} and S_n^{2-} is same, it suggests that S^{2-} was primarily oxidized to $S_2O_3^{2-}$ through the reduction of aqueous SeO_3^{2-} to zero-valent Se (SeS_2 and Se^0). The increase of solid S_n^{2-} observed in S_{2p} XPS spectra suggests the formation of an intermediate amorphous solid phase $Fe_2^{III}Fe^{II}S_4$ (later transformed to pyrite), which could account for Fe(III) species in Fe($2p_{3/2}$) XPS part.[46-48] Finck et al. reported that sulfide, instead of Fe(II), contributed to the reduction of SeO_3^{2-}, as indicated by the detection of FeS_2 by XRD.[19] Here, it should be noted as the content of Se-sorbed was quite lower than the mass of solid matrix and the primary Se XPS region is 3d, the interference of Se $3p_{3/2}$ (161.7 eV) could be neglected. After 73h, the percentage of $S_2O_3^{2-}$ peak area increased to 40.5% and 10.8% of S^0 species were also detected. In contrast, the percentages of S^{2-} and S_n^{2-} contributions decreased to 27.1% and 21.5%, respectively, suggesting that S^{2-} and S_n^{2-} were oxidized to $S_2O_3^{2-}$ and S^0 (equation 5 and 6). From 73h to 192h, more S_n^{2-} was oxidized to $S_2O_3^{2-}$, which should be responsible for the reduction of SeO_3^{2-}. Usually, the oxidation of S^{2-} followed S^{2-}- S_n^{2-} - S^0 pathway during Se(VI) reduction and more than 90% of S^{2-}/S_n^{2-} was oxidized to S^0 with little amount of $S_2O_3^{2-}$ and SO_4^{2-} at acid or weakly alkaline conditions.[45,49] In the present study, $S_2O_3^{2-}$ was the only oxidation product after 192 h reaction with Se(IV). The summed concentration of S^{2-}/S_n^{2-}, SO_3^{2-} and SO_4^{2-} is almost the same value of the total S (Figure 4),

indicating that Se(VI)-sorbed onto mackinawite was reduced by solid S^{2-}, not by aqueous S^{2-} species even though plenty of aqueous S^{2-}/S_n^{2-} were present in solution. The reduction mechanism is not totally consistent with the one reported for U(VI) reduction by FeS by Hua et al, who found U(VI)-sorbed to be reduced by either S^{2-}-solid or dissolved HS^-.[50] A direct reduction of Se(IV) by aqueous S^{2-} was shown to be the dominant reaction at low initial pH.[19] Probably aqueous solid S^{2-} was more reactive for the reduction of Se(IV) than aqueous S^{2-} in CPW. Aqueous S^{2-} was stabled at pH 12.2 under reducing conditions for a long time.[51]

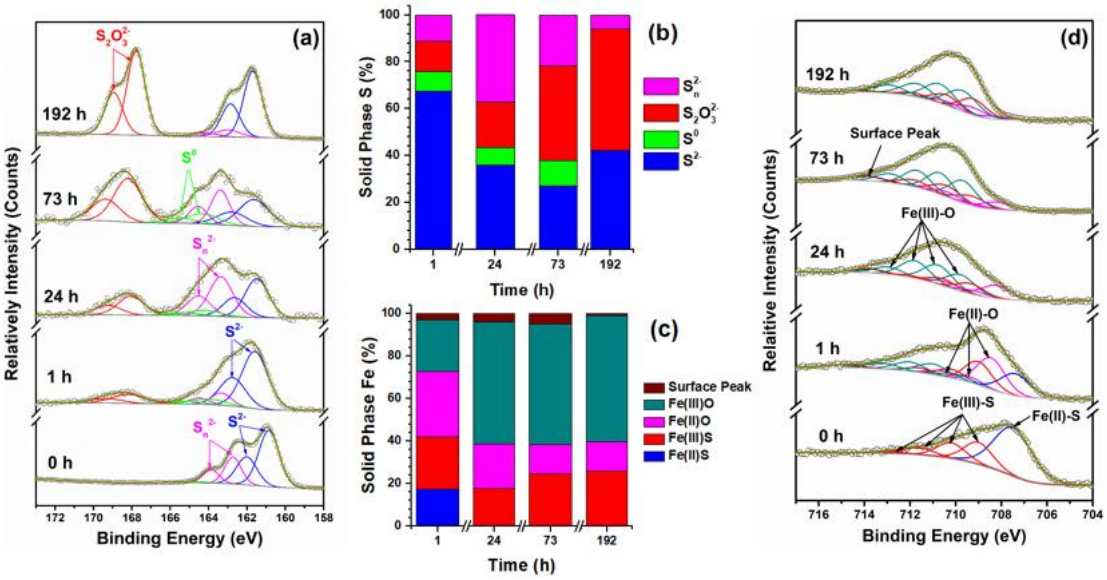

Figure 5. XPS spectra (a) narrow S(2p) and (d) Fe($2p_{3/2}$) (d) XPS scan, and the fractions of corresponding components of (b) S and (c) Fe species. Circles were experimental data; bottom solid line was the Shirley background; dashed lines were the fit to each spectrum and top solid line was the sum of background and fitted peaks.

The broad Fe($2p_{3/2}$) spectrum of mackinawite (Figure 5d, 0 h reaction time) could be fitted by one Fe(II)-S peak at ~707.5 eV and one main peak of Fe(III)-S at 709.1 eV with three multiple peaks.[41] The area ratio of each multiple peak to the first Fe(III)-S component is equal to 0.66, 0.31, and 0.10 respectively, in good agreement with other studies on mackinawite.[42] The Fe($2p_{3/2}$) peaks fitted in the current study are listed in

Table S9. Compared with the XPS result of pristine mackinawite, three multiple peaks of Fe(II)-O and four multiple peaks of Fe(III)-O were observed in the Fe 2p spectrum of SeO_3^{2-}-reacted mackinawite at 1 h. This suggests the oxidation of Fe(II) to Fe(III) (equation 7), coupled to SeO_3^{2-} reduction (equation 1). Also, the Fe(II) hydroxyl-complexes are important in alkaline solution and $Fe(OH)_2$ is probably formed. An increased (33.2%) Fe(III)-O peak intensity and an absence of Fe(II)-S peak are observed after 24 h reaction compared with the 1 h sample, which was probably related to the oxidation of Fe(II) and the further release S^{2-} by the solid. The XPS peak of S^{2-} to be show in Figure 5a at 24 h may be attributed to Fe(III)-S species. Similar results of Fe(II) oxidation to Fe(III) were observed in mackinawite reacted with Se (IV) at different pH values.[25,40] As reaction time increased to 73 h, the content of Fe(III)-O remained constant, indicating that no more SeO_3^{2-} was reduced by Fe(II). Mixtures of Fe(II)-O and Fe(III)-O observed on the solid surface may imply a formation of multi-valent iron (oxyhydr)oxides such as green rust, magnetite, or other phases containing both ferrous and ferric sites.[52] Furthermore, the presence of Fe(III)-S species was probably due to the transformation of FeS to amorphous $Fe_2^{III}Fe^{II}S_4$ resulting in the enrichment of S combined with Fe(III) or/and the formation of $Fe^{III}S_2O_3^+$ species via Se reduction. Lan et al. suggested that Fe_3S_4 was present beneath Fe(III) (hydr)oxide precipitation during FeS transformation at pH 8.[53]

The XRD patterns of 50 and 192 h solid samples show a poor crystallinity and differed from the original mackinawite in Figure S7. The XRD pattern from the 50 h sample probably indicated that the formation of poor crystallized Fe_3S_4 and $Fe(OH)_3$, in agreement with the XPS results. The very broad XRD reflections in 192 h sample is attributed to magnetite and $Fe(OH)_3$ with very poor crystallinity. Normalized Fe K-edge XANES spectra of the 192 h solid sample and of the references, including mackinawite, magnetite, and hematite, are shown in Figure S11, together with the LCF result. The result shows that the species present in the solid product was similar to magnetite, in good accordance with black color of the filtrate at 192 h.

Furthermore, the ratio of Fe(II)-O/Fe(III)-O identified by XPS at 192 h was 0.23, less than the idea value of 0.5, and the presence of Fe(III)-S species suggested the final solid contained amorphous $Fe(OH)_3$ and $FeS_2O_3^+$ complexed to Cl^- or OH^- species except very poor crystallization magnetite. The Eh-pH diagram of Fe species shown in Figure S9b indicated that mackinawite tends to dissolve and to form magnetite. It is well known that $Fe(OH)_2$, an extremely redox-sensitive phase in solution, could lead via the Shikorr reaction[54] to a disproportion reaction to magnetite under anaerobic condition. Furthermore, the interaction of SeO_3^{2-} with Fe(II) could produce Se^0 and metastable green rust (GR), which is know to have the potential to reduce SeO_3^{2-} to Se^0 via being oxidized to magnetite.[55]

4. Environmental relevance

It is critical to waste depository safety to improve our understanding of reductive precipitation of mobile radionuclides in hyperalkaline conditions, and specifically to measure the surface complexes, aqueous speciation and solubility in order to decipher immobilization pathways and the underlying interaction mechanisms when contaminations are in contact with cement media.[56] Mackinawite, as one of the steel corrosion products and one of the common naturally-occurring iron sulfides, showed an extremely high sorption and reduction ability towards SeO_3^{2-} within a relatively short interaction time (~96 hours). SeO_3^{2-} can be reduced to a mixture of SeS_2 and Se^0 solid species, as confirmed by Se K-edge XAS. However, the zero-valent selenium species shows a relatively high solubility and thus mobility in CPW, with ~99% of reduction products released to the solution in the form of Se_4S nanoparticles confirmed by TEM-EDS after 192 hours. The surface chemistry of the mackinawite evolved during the reaction in the following wasy: 2 to 3 S^{2-}/S_n^{2-} units were substituted by one SeO_3^{2-} atom. 62% of initial solid S^{2-}/S_n^{2-} was released into solution when in presence of SeO_3^{2-} and mackinawite was transformed to magnetite, $Fe(OH)_3$ and $FeS_2O_3^+$ complexed to Cl^- or OH^- species after 192 h. The current study provides

valuable information about the reduction mechanisms of redox-sensitive radionuclides in presence of iron sulfides that have strongly reduction capacity.

ASSOCIATED CONTENT

Supporting Information Available. Additional materials referenced in the text are available free of charge.

The composition of CPW. XRD patterns, and TEM micrograph of synthesized mackinawite. The calibration curves of SO_4^{2-}, SO_3^{2-},S^{2-}/S_n^{2-}, SeO_3^{2-} and the relative retention time of the ions. Picture of the filtrate color. Se K-edge EXAFS of solid samples. STEM image and EDS mapping results of solid sample. Se and Fe species Eh-pH diagrams. Aqueous concentration of SO_4^{2-}, SO_3^{2-},S^{2-}/S_n^{2-} in the filtrate. Binding energies (BE), Peak full width at half maximum (FWHM) and peak areas for S(2p) and Fe($2p_{3/2}$). Fe K-edge normalized XANES spectra and LCF result of solid samples.

AUTHOR INFORMATION

Corresponding Authors

*Phone: +33(0) 6 75 87 82 66. E-mail: charlet38@gmail.com (Laurent Charlet)

*Phone: +33(0) 7 67 13 83 83. E-mail: bin.ma@psi.ch (Bin Ma).

Notes

The authors declare no competing financial interest.

Acknowledgements

The authors would like to thank ANDRA (Agence Nationale pour la gestion des Déchets Radioactifs, Châtenay-Malabry) for project funding and laboratory equipment related to this work. L. Charlet is grateful to the National Research Council (CNRS), France, for providing partial financial support for this work. Kaifeng Wang and Bin Ma also thanks China Scholaship Council(CSC) for financial support.

The synchrotron facility ALBA is acknowledge for the allocation for the beamlime (proposal 2019093916).

Reference

1. Kausch, M. F.; Pallud, C. E., Modeling the impact of soil aggregate size on selenium immobilization. *Biogeosciences* **2013,** *10*, (3), 1323-1336.
2. Breynaert, E.; Bruggeman, C.; Maes, A., XANES-EXAFS analysis of se solid-phase reaction products formed upon contacting Se(IV) with FeS2 and FeS. *Environ. Sci. Technol.* **2008,** *42*, (10), 3595-3601.
3. Bruggeman, C.; Maes, A.; Vancluysen, J.; Vandenmussele, P., Selenite reduction in Boom clay: Effect of FeS2, clay minerals and dissolved organic matter. *Environ. Pollut.* **2005,** *137*, (2), 209-221.
4. Charlet, L.; Scheinost, A. C.; Tournassat, C.; Greneche, J. M.; Gehin, A.; Fernandez-Martinez, A.; Coudert, S.; Tisserand, D.; Brendle, J., Electron transfer at the mineral/water interface: Selenium reduction by ferrous iron sorbed on clay. *Geochim. Cosmochim. Acta* **2007,** *71*, (23), 5731-5749.
5. Sun, W. L.; Renew, J. E.; Zhang, W. L.; Tang, Y. Z.; Huang, C. H., Sorption of Se(IV) and Se(VI) to coal fly ash/cement composite: Effect of Cat(2+) and high ionic strength. *Chem. Geol.* **2017,** *464*, 76-83.
6. Ma, B.; Fernandez-Martinez, A.; Wang, K. F.; Made, B.; Henocq, P.; Tisserand, D.; Bureau, S.; Charlet, L., Selenite Sorption on Hydrated CEM-V/A Cement in the Presence of Steel Corrosion Products: Redox vs Nonredox Sorption. *Environ. Sci. Technol.* **2020,** *54*, (4), 2344-2352.
7. Bonhoure, I.; Baur, I.; Wieland, E.; Johnson, C. A.; Scheidegger, A. M., Uptake of Se(IV/VI) oxyanions by hardened cement paste and cement minerals: An X-ray absorption spectroscopy study. *Cem. Concr. Res.* **2006,** *36*, (1), 91-98.
8. Onoguchi, A.; Granata, G.; Haraguchi, D.; Hayashi, H.; Tokoro, C., Kinetics and mechanism of selenate and selenite removal in solution by green rust-sulfate. *R. Soc. Open Sci.* **2019,** *6*, (4).
9. Xu, L.; Huang, Y. H., Kinetics and mechanism of selenite reduction by zero valent iron under anaerobic condition activated and enhanced by dissolved Fe(II). *Sci. Total Environ.* **2019,** *664*, 698-706.
10. Scheinost, A. C.; Charlet, L., Selenite reduction by mackinawite, magnetite and siderite: XAS characterization of nanosized redox products. *Environ. Sci. Technol.* **2008,** *42*, (6), 1984-1989.
11. Wu, J.; Zeng, R. J., In Situ Preparation of Stabilized Iron Sulfide Nanoparticle-Impregnated Alginate Composite for Selenite Remediation. *Environ. Sci. Technol.* **2018,** *52*, (11), 6487-6496.
12. Wu, J.; Zhao, J.; Li, H.; Miao, L. Z.; Hou, J.; Xing, B. S., Simultaneous Removal of Selenite and Selenate by Nanosized Zerovalent Iron in Anoxic Systems: The Overlooked Role of Selenite. *Environ. Sci. Technol.* **2021,** *55*, (9), 6299-6308.
13. Ma, B.; Charlet, L.; Fernandez-Martinez, A.; Kang, M.; Made, B., A review of the retention mechanisms of redox-sensitive radionuclides in multi-barrier systems. *Appl. Geochem.* **2019,** *100*, 414-431.

14. Kirsch, R.; Fellhauer, D.; Altmaier, M.; Neck, V.; Rossberg, A.; Fanghanel, T.; Charlet, L.; Scheinost, A. C., Oxidation State and Local Structure of Plutonium Reacted with Magnetite, Mackinawite, and Chukanovite. *Environ. Sci. Technol.* **2011,** *45*, (17), 7267-7274.
15. Yalcintas, E.; Scheinost, A. C.; Gaona, X.; Altmaier, M., Systematic XAS study on the reduction and uptake of Tc by magnetite and mackinawite. *Dalton Trans.* **2016,** *45*, (44), 17874-17885.
16. Wharton, M. J.; Atkins, B.; Charnock, J. M.; Livens, F. R.; Pattrick, R. A. D.; Collison, D., An X-ray absorption spectroscopy study of the coprecipitation of Tc and Re with mackinawite (FeS). *Appl. Geochem.* **2000,** *15*, (3), 347-354.
17. Zhou, J. M.; Chen, S.; Liu, J.; Frost, R. L., Adsorption kinetic and species variation of arsenic for As(V) removal by biologically mackinawite (FeS). *Chem. Eng. J.* **2018,** *354*, 237-244.
18. Jeong, H. Y.; Klaue, B.; Blum, J. D.; Hayes, K. F., Sorption of mercuric ion by synthetic manocrystalline mackinawite (FeS). *Environ. Sci. Technol.* **2007,** *41*, (22), 7699-7705.
19. Finck, N.; Dardenne, K., Interaction of selenite with reduced Fe and/or S species: An XRD and XAS study. *J. Contam. Hydrol.* **2016,** *188*, 44-51.
20. Jung, B.; Safan, A.; Batchelor, B.; Abdel-Wahab, A., Spectroscopic study of Se(IV) removal from water by reductive precipitation using sulfide. *Chemosphere* **2016,** *163*, 351-358.
21. Mace, N.; Nerfie, P.; Nathalie Coreau, N.; Thory, E.; Bescop. L. P.; Touze. G.; Spécifications techniques: Préparation et caractérisations des PCH CEM V/A ROMBAS dans le cadre du GL CTEC DPC/SECR/ST/2015/057 indice A. **2015**.
22. Markelova, E.; Parsons, C. T.; Couture, R.-M.; Smeaton, C. M.; Madé, B.; Charlet, L.; Van Cappellen, P. Deconstructing the redox cascade: what role do microbial exudates (flavins) play?. *Environ. Chem.* **2017**, 14 (8), 515– 524.
23. Ravel, B.; Newville, M., ATHENA, ARTEMIS, HEPHAESTUS: data analysis for X-ray absorption spectroscopy using IFEFFIT. J. of Synchrotron Radiat. 2005, 12, 537-541.
24. Ankudinov, A. L.; Ravel, B.; Rehr, J. J.; Conradson, S. D. Real-space multiple-scattering calculation and interpretation of x-ray-absorption near-edge structure. *Phys. Rev. B: Condens. Matter Mater. Phys.* **1998**, 58 (12), 7565– 7576.
25. Han, D. S.; Batchelor, B.; Abdel-Wahab, A., Sorption of selenium(IV) and selenium(VI) to mackinawite (FeS): Effect of contact time, extent of removal, sorption envelopes. *J. Hazard. Mater.* **2011,** *186*, (1), 451-457.
26. Mitchell, K.; Couture, R. M.; Johnson, T. M.; Mason, P. R. D.; Van Cappellen, P., Selenium sorption and isotope fractionation: Iron(III) oxides versus iron(II) sulfides. *Chem. Geol.* **2013**, 342, 21-28.
27. Giffaut, E.; Grive, M.; Blanc, P.; Vieillard, P.; Colas, E.; Gailhanou, H.; Gaboreau, S.; Marty, N.; Made, B.; Duro, L., Andra thermodynamic database for performance assessment: ThermoChimie. *Appl. Geochem.* **2014,** *49*, 225-236.

28. Ma, B.; Fernandez-Martinez, A.; Mancini, A.; Lothenbach, B., Spectroscopic investigations on structural incorporation pathways of Fe-III into zeolite frameworks in cement-relevant environments. *Cem. Concr. Res.* **2021**, 140.
29. Kang, M. L.; Ma, B.; Bardelli, F.; Chen, F. R.; Liu, C. L.; Zheng, Z.; Wu, S. J.; Charlet, L., Interaction of aqueous Se(IV)/Se(VI) with FeSe/FeSe2: Implication to Se redox process. *J. Hazard. Mater.* **2013**, 248, 20-28.
30. Diener, A.; Neumann, T.; Kramar, U.; Schild, D., Structure of selenium incorporated in pyrite and mackinawite as determined by XAFS analyses. *J. Contam. Hydrol.* **2012,** *133*, 30-39.
31. Geoffroy, N.; Demopoulos, G. P., The elimination of selenium(IV) from aqueous solution by precipitation with sodium sulfide. *J. Hazard. Mater.* **2011,** *185*, (1), 148-154.
32. Sasaki, K.; Blowes, D. W.; Ptacek, C. J., Spectroscopic study of precipitates formed during removal of selenium from mine drainage spiked with selenate using permeable reactive materials. *Geochem. J.* **2008,** *42*, (3), 283-294.
33. Prasad, K. S.; Vaghasiya, J. V.; Soni, S. S.; Patel, J.; Patel, R.; Kumari, M.; Jasmani, F.; Selvaraj, K., Microbial Selenium Nanoparticles (SeNPs) and Their Application as a Sensitive Hydrogen Peroxide Biosensor. *Appl. Biochem. Biotechnol.* **2015,** *177*, (6), 1386-1393.
34. Zhenghua, W.; Shiyu, Z. H. U., Rapid growth of t-Se nanowires in acetone at room temperature and their photoelectrical properties. *Front. Optoelectron. China* **2011,** *4*, (2), 188-194.
35. Turgeman, R.; Gedanken, A., Crystallization of ZnO on crystalline magnetite nanoparticles in the presence of ultrasound radiation. *Cryst. Growth Des.* **2006**, 6, (10), 2260-2265.
36. Wolthers, M.; Charlet, L.; Van der Linde, P. R.; Rickard, D.; Van der Weijden, C. H., Surface chemistry of disordered mackinawite (FeS). *Geochim. Cosmochim. Acta* **2005,** *69*, (14), 3469-3481.
37. Lothenbach, B.; Rentsch, D.; Wieland, E., Hydration of a silica fume blended low-alkali shotcrete cement. *Phys. Chem. Earth* **2014**, 70-71, 3-16.
38. Beat M., Chapter 3-Properties. *Sulfur, Energy, and Environment.* **1997**, 38-116.
39. Han, D. S.; Batchelor, B.; Abdel-Wahab, A., Sorption of selenium(IV) and selenium(VI) onto synthetic pyrite (FeS2): Spectroscopic and microscopic analyses. *J. Colloid Interface Sci.* **2012**, 368, 496-504.
40. Scheinost, A. C.; Kirsch, R.; Banerjee, D.; Fernandez-Martinez, A.; Zaenker, H.; Funke, H.; Charlet, L., X-ray absorption and photoelectron spectroscopy investigation of selenite reduction by Fe-II-bearing minerals. *J. Contam. Hydrol.* **2008**, 102, (3-4), 228-245.
41. Herbert, R. B.; Benner, S. G.; Pratt, A. R.; Blowes, D. W., Surface chemistry and morphology of poorly crystalline iron sulfides precipitated in media containing sulfate-reducing bacteria. *Chem. Geol.* **1998,** *144*, (1-2), 87-97.

42. Mullet, M.; Boursiquot, S.; Abdelmoula, M.; Genin, J. M.; Ehrhardt, J. J., Surface chemistry and structural properties of mackinawite prepared by reaction of sulfide ions with metallic iron. *Geochim. Cosmochim. Acta* **2002,** *66*, (5), 829-836.
43. Matamoros-Veloza, A.; Cespedes, O.; Johnson, B. R. G.; Stawski, T. M.; Terranova, U.; de Leeuw, N. H.; Benning, L. G., A highly reactive precursor in the iron sulfide system. *Nat. Commun.* **2018**, 9.
44. Beauvais, M. L.; Chupas, P. J.; O'Nolan, D.; Parise, J. B.; Chapman, K. W., Resolving Single-layer Nanosheets as Short-lived Intermediates in the Solution Synthesis of FeS. *ACS Mater. Lett.* **2021,** *3* (6), 698-703.
45. Kang, M. L.; Bardelli, F.; Ma, B.; Charlet, L.; Chen, F. R.; Yang, Y. Q., The influence of pH and reaction time on the formation of FeSe2 upon selenite reduction by nano-sized pyrite-greigite. *Radiochim. Acta* **2016,** *104* (9), 649-656.
46. Benning, L. G.; Wilkin, R. T.; Barnes, H. L., Reaction pathways in the Fe-S system below 100 degrees C. *Chemical Geology* **2000,** *167* (1-2), 25-51.
47. Hunger, S.; Benning, L. G., Greigite: a true intermediate on the polysulfide pathway to pyrite. *Geochemical Trans.* **2007,** *8*.
48. Bourdoiseau, J. A.; Jeannin, M.; Remazeilles, C.; Sabota, R.; Refait, P., The transformation of mackinawite into greigite studied by Raman spectroscopy. *J. Raman Spectrosc.* **2011,** *42* (3), 496-504.
49. Ma, B.; Kang, M. L.; Zheng, Z.; Chen, F. R.; Xie, J. L.; Charlet, L.; Liu, C. L., The reductive immobilization of aqueous Se(IV) by natural pyrrhotite. *J. Hazard. Mater.* **2014,** *276*, 422-432.
50. Hua, B.; Deng, B. L., Reductive Immobilization of Uranium(VI) by Amorphous Iron Sulfide. *Environ. Sci. Technol.* **2008,** *42* (23), 8703-8708.
51. Lothenbach, B.; Le Saout, G.; Ben Haha, M.; Figi, R.; Wieland, E., Hydration of a low-alkali CEM III/B-SiO2 cement (LAC). *Cem. Concr. Res.* **2012,** *42* (2), 410-423.
52. Han, D. S.; Batchelor, B.; Abdel-Wahab, A., XPS analysis of sorption of selenium(IV) and selenium(VI) to mackinawite (FeS). *Environ. Prog. Sustain. Energy* **2013,** *32*, (1), 84-93.
53. Lan, Y.; Butler, E. C., Iron-Sulfide-Associated Products Formed during Reductive Dechlorination of Carbon Tetrachloride. *Environ. Sci. Technol.* **2016,** *50* (11), 5489-5497.
54. Ma, M.; Zhang, Y.; Guo, Z. R.; Gu, N., Facile synthesis of ultrathin magnetic iron oxide nanoplates by Schikorr reaction. *Nanoscale Res. Lett.* **2013,** *8*, 1-7.
55. Borsig, N.; Scheinost, A. C.; Shaw, S.; Schild, D.; Neumann, T., Retention and multiphase transformation of selenium oxyanions during the formation of magnetite via iron(II) hydroxide and green rust. *Dalton Trans.* **2018,** *47*, (32), 11002-11015.
56. Altmann, S., 'Geo'chemical research: A key building block for nuclear waste disposal safety cases. *J. Contam. Hydrol.* **2008,** *102*, (3-4), 174-179.